Supporting Information

Poincloux et al. 10.1073/pnas.1010396108

SI Methods

Cell Culture, Inhibitors, and siRNA Treatments. MDA-MB-231 human breast adenocarcinoma cells (ATCC #HTB-26) and stable line of MDA-MB-231 cells expressing mCh-Lifeact (1, 2) were maintained in L-15 culture medium (Sigma-Aldrich) with 2 mM Glutamine and 15% FCS, at 37 °C and 1% CO_2.

Rho inhibitor C3 exoenzyme (Sigma-Aldrich) was used at 1 μg/mL, and ROCK inhibitor Y27632 (Calbiochem) was used at 10 μM. Blebbistatin (Tocris Bioscience), a myosin II inhibitor, was used at 50 μM. MMP inhibitor GM6001 (Chemicon) was used at 20 μM. Anti-human β1 integrin mouse mAb 4B4 (Beckman Coulter) was used to block β1 integrin (2 μg/mL) (3). Mouse monoclonal anti-sheep red blood cells IgG (ATCC #TIB-111) was used as a control in experiments using 4B4 mAb. Nonpeptide RGD mimetic, compound S36578-2 (1 μM), described as a highly selective inhibitor for αv (β3 and β5) integrins (4), was a gift of G.C. Tucker (Servier Research Institute, Croissy-sur-Seine, France). General inhibitor of formin homology 2 domains (SMIFH2; ref. 5) was used at 25 μM and was a gift of M.H. Verlhac (Pierre et Marie Curie Université, Paris).

For siRNA treatment, cells were transfected with Oligofectamine (Invitrogen) according to manufacturer's instructions. The following siRNAs were used:

ON-TARGETplus (Dharmacon):

siRhoA-a (10 nM): CGACAGCCCUGAUAGUUUAUU;
siRhoA-b (10 nM): GACCAAAGAUGGAGUGAGAUU;
sip34-a (10 nM): CCAUGUAUGUUGAGUCUAAUU;
sip34-b (10 nM): GGACAGAGUCACAGUAGUCUU;
siβ1-a (50 nM): GUGCAGAGCCUUCAAUAAA, GGUA GAAAGUCGGGACAAA, UGAUAGAUCCAAUG GCUUA, GGGCAAACGUGUGAGAUGU (Smartpool).
HP GenomeWide siRNA (QIAGEN):
siβ1-b (50 nM): AAGUCUUGGAACAGAUCUGTT.
Cells were analyzed 72 h after treatment.

Antibodies. Rabbit polyclonal antibodies against nonmuscle myosin II heavy chain A were obtained from Covance. Rabbit polyclonal anti-phospho-Myosin Light Chain 2 (Ser19) antibodies were purchased from Cell Signaling. Mouse mAb against Golgi marker CTR433 was a gift from M. Bornens (Institut Curie, Paris). Monoclonal anti-RhoA was provided by J. Bertoglio (Institut National de la Santé et de la Recherche Médicale U461, Chatenay Malabry, France). Mouse anti-p16-Arc and p34-Arc mAbs were purchased from Synaptic Systems. Anti-β1 integrin rabbit polyclonal antibodies were provided by C. Albiges-Rizo (Institut Albert Bonniot, Grenoble, France). Cy3-conjugated AffiniPure F(ab′)2 fragment donkey anti-mouse or anti-rabbit IgGs were from Jackson ImmunoResearch Laboratories.

Indirect Immunofluorescence Analysis. For immunofluorescence analysis, MDA-MB-231 cells were included for 4 h in Matrigel (9–11 mg/mL; BD Biosciences). Then, cells were pre-extracted with 0.3% Triton-X100 in 4% PFA for 90 s, fixed with 4% PFA in PBS for 20 min, quenched with 50 mM NH_4Cl for 10 min and blocked with 5% FCS in PBS for 20 min. Samples were incubated with antibodies or Alexa Fluor-labeled phalloidin (Invitrogen) in PBS for 1 h, washed with PBS, and air-dried before mounting in Prolong Gold Antifade reagent containing DAPI (Invitrogen). Cells were examined under a motorized upright wide-field microscope (Leica DMRA2) with oil immersion ×100 PL APO HCX, 1.4 NA with Z positioning accomplished using a piezoelectric driver (Physik Instrument) mounted underneath the objective lens and a cooled interlined CCD CoolSNAP HQ camera (Photometrics) driven by MetaMorph 6 (Molecular Devices). Stacks of images were taken at 0.2-μm increments along the *z* axis. Except for Fig. S3 and Movie S8, stacks were deconvoluted by the 3D Deconvolution Metamorph module with the fast iterative constrained PSF-based algorithm (6). For Fig. S1*C* and Movie S3, images were recorded at 0.3-μm increments using the ×100 objective mounted on a PIFOC objective stepper of a DM IRE2 microscope (Leica Microsystems) equipped with a Cascade II camera (Photometrics) and processed for deconvolution.

For quantitative analyses shown in Figs. 4 *A* and *B* and 5*A*, fluorescence intensity profile along the cell cortex was measured on the cell equatorial plane from nondeconvoluted images with ImageJ software. Profile length was centered on F-actin intensity maximum (position 0) and normalized (−1 to +1). After subtraction of background signal measured outside the cell, intensity profile was normalized to 1 and interpolated. Normalized profiles from 15 cells were averaged.

Spinning Disk Confocal Microscopy. Images were recorded at 0.3-μm increments using a Nikon Eclipse TE2000-U microscope equipped with a ×100 1.45 NA objective, a PIFOC objective stepper, a Yokogawa CSU22 confocal unit, and a CoolSNAP HQ^2 camera (Photometrics) driven by MetaMorph 6. Cell repositioning and kymograph analysis were performed with ImageJ plugin StackReg (P. Thévenaz, Swiss Federal Institute of Technology, Lausanne, Switzerland) and Kymograph (J. Rietdorf and A. Seitz, European Molecular Biology Laboratory, Heidelberg, Germany).

Analysis of Matrix Displacements by PIV. Yellow-green fluorescent carboxylate-modified microbeads (0.2-μm diameter; Molecular Probes) were resuspended in PBS and mixed with Matrigel (1/50 vol/vol) at 1.8×10^{12} beads per mL final concentration on ice to prevent polymerization. Control, drug-, or siRNA-treated MDA-MB-231 cells expressing mCh-Lifeact were included in 50 μL of Matrigel containing microbeads at a concentration of 2×10^6 cells per mL, dropped on the surface of an Iwaki glass-bottom dish (Sterilin Limited), and left to polymerize in a humidified atmosphere at 37 °C and 1% CO_2 for 30 min before addition of culture medium. Images of mCh-Lifeact and fluorescent microbeads were recorded with the ×60 1.4 NA objective of an automated Nikon TE2000-E microscope equipped with a CoolSNAP HQ camera driven by MetaMorph 6.

Stacks consisting of seven optical sections separated by 2-μm step around the cell equatorial plane were acquired every 15 min over 4 h. To allow representative sampling of the different cell populations, ∼40 fields per condition and experiment were recorded. Two optical sections corresponding to the cell's equatorial plane were projected and used for analysis of bead movement by PIV, which consists of extracting the local displacement vectors from the cross-correlation of successive images (7). Analyzing matrix deformations inside Matrigel was facilitated by the simple and constant MDA-MB-231 cell geometry and symmetry that allowed reducing the field of observation to the cell equatorial plane without taking into account matrix movements on the *z* axis. Stacks of microbead images were analyzed by using a customized MatLab software (MathWorks, Inc.) based on the MatPIV package (J.K. Sveen, University of Oslo, Sweden; available at http://www.math.uio.no/~jks/matpiv/).

After masking out the region where the cell dwells, we ran the PIV computation with a cross-correlation window size of 32 or

64 pixels with no noticeable difference. For each cell, a temporal average velocity field was computed after registration of each image of a time series (4 h) to place the mass center of the cell in the center and a rotation of the field so that the speed vector of cell migration is aligned horizontally to the right. For each condition, the individual velocity fields of several cells were averaged (code available upon request). The amplitude of the bead velocity was color-coded, and the direction of displacements was depicted with arrows.

Scanning Electron and Transmission Electron Microscopy. For scanning electron microscopy observations of cell invasion through Matrigel, the upper chamber of a Transwell cell culture insert (BD Biosciences) was filled with 100 μL of Matrigel and the lower chamber with L15 medium containing 15% FCS. Cells were serum-starved for 2 h and added on top of the Matrigel layer in serum-free L15 medium. Samples were fixed at different time points with 2.5% glutaraldehyde in 0.1 M cacodylate buffer (pH 7.4) overnight at 4 °C. Preparations were then washed three times for 5 min in 0.2 M cacodylate buffer (pH 7.4), postfixed for 1 h in 1% (wt/vol) osmium tetroxide in 0.2 M cacodylate buffer (pH 7.4), and rinsed with distilled water. Samples were dehydrated through a graded series (25–100%) of ethanol, transferred in acetone and subjected to critical point drying with CO_2 in a Balzers CPD 030. Dried specimens were sputter-coated with gold with a BALTEC MED 010 evaporator and were examined and photographed with a JEOL JSM 6700F field emission scanning electron microscope operating at 10 kV. Images were acquired from the upper SE detector and pseudocolored with Photoshop software. Cell invasion was determined by analyzing the proportion of cells buried in Matrigel after 14 h from low-magnification micrographs taken from the center of the transwell to avoid edge effect.

For transmission electron microscopy, 10^5 MDA-MB-231 cells were included for 4 h in 25 μL of Matrigel. Cells were fixed with 2.5% glutaraldehyde in 0.1 M cacodylate buffer (pH 7.4), postfixed with 2% OsO_4/1.5% potassium ferrocyanure, dehydrated in ethanol, and embedded in Epon. Thin sections (~60 nm) were cut using a Reichert Ultracut-E Microtome (Leica Microsystems) and placed on formvar-coated grids. Sections on grids were contrasted for 4 min with 2% uranyl acetate in 70% methanol and 1 min in lead citrate. Observations were made under a Philips CM120 transmission electron microscope (FEI Company), and digital acquisitions were performed with a KeenView camera (Olympus Soft Imaging Solutions).

1. Riedl J, et al. (2008) Lifeact: A versatile marker to visualize F-actin. *Nat Methods* 5: 605–607.
2. Lizárraga F, et al. (2009) Diaphanous-related formins are required for invadopodia formation and invasion of breast tumor cells. *Cancer Res* 69:2792–2800.
3. Matsuyama T, et al. (1989) Activation of CD4 cells by fibronectin and anti-CD3 antibody: A synergistic effect mediated by the VLA-5 fibronectin receptor complex. *J Exp Med* 170:1133–1148.
4. Maubant S, et al. (2006) Blockade of alpha v beta3 and alpha v beta5 integrins by RGD mimetics induces anoikis and not integrin-mediated death in human endothelial cells. *Blood* 108:3035–3044.
5. Rizvi SA, et al. (2009) Identification and characterization of a small molecule inhibitor of formin-mediated actin assembly. *Chem Biol* 16:1158–1168.
6. Sibarita JB (2005) Deconvolution microscopy. *Adv Biochem Eng Biotechnol* 95: 201–243.
7. Raffel M, Willert CE, Wereley ST, Kompenhans J (2007) *Particle Image Velocimetry: A Practical Guide* (Springer, Berlin), 2nd Ed.

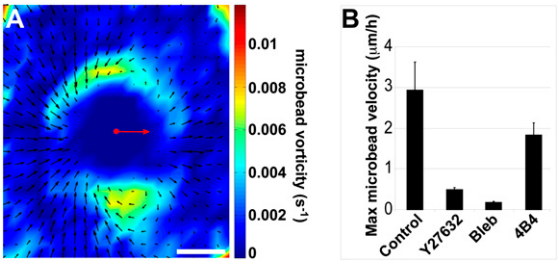

Fig. S1. Visualization of high shear motion of the Matrigel on the sides of the cells. (*A*) Vorticity $\omega = \nabla \times \mathbf{u}$ computed from second-ordered centered differences from the averaged velocity field (Fig. 1*B*) is shown on the color-coded background, emphasizing the high shear motion of the Matrigel on the side of the cells. While cells are moving to the right, they exert large tractions on the matrix to pull it toward their rear, thus displaying high shear motions on their sides. (Scale bar, 10 μm.) (*B*) Matrigel maximum displacements computed from temporal averaged PIV measurements in control condition (n = 8 cells; Fig. 1*B*), ROCK inhibition (n = 13 cells; Fig. 4*D*), Myosin II inhibition (n = 4 cells; Fig. 4*E*) and β1 integrin inhibition with 4B4 blocking antibody (n = 7 cells; Fig. 5*E*). The increase of maximum displacements in the β1 integrin inhibition condition compared with ROCK or myosin II inhibition conditions is due to the spatially random blebbing activity that induces large local displacements of the Matrigel, although those displacements did not appear on PIV average map because of spatial averaging.

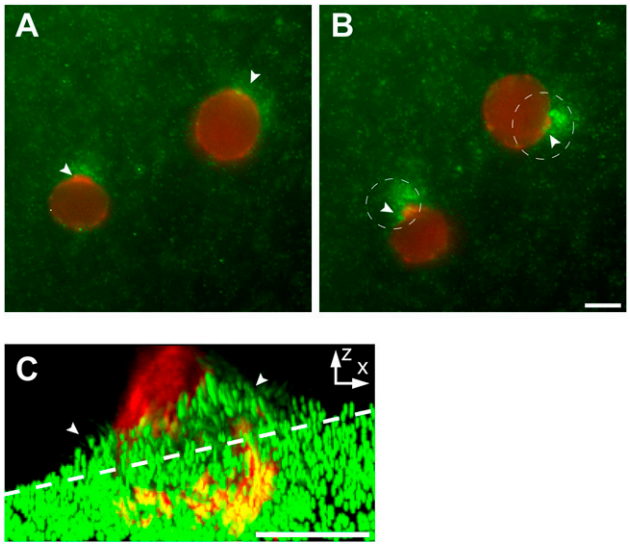

Fig. S2. Visualization of Matrigel remodeling with seeded fluorescent microbeads. (*A* and *B*) Movement of MDA-MB-231 cells stably expressing the F-actin probe mCh-Lifeact (red) within 3D Matrigel seeded with fluorescent microbeads (green) was analyzed by live-cell imaging. The first (*A*) and last time frame (*B*) of a time-lapse sequence (4 h apart) are shown (Movie S2). Initial position of the cells is underlined in *B*. Note accumulation of beads at the cell rear coinciding with the region of F-actin accumulation (arrowheads). (*C*) mCh-Lifeact MDA-MB-231 cells plated atop a thick layer of Matrigel seeded with fluorescent microbeads were incubated for 4 h and a stack of optical sections was taken along the *z* axis. The image is a maximum intensity projection along the *y* axis. The dashed line indicates the surface of the cell-free region of the matrix. (Scale bars, 10 μm.)

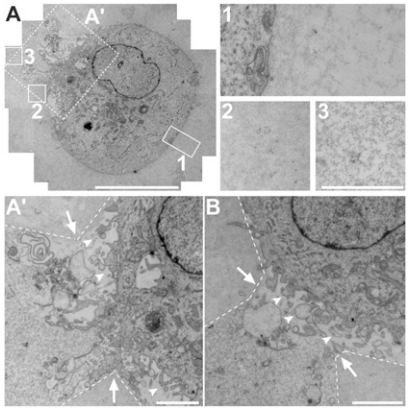

Fig. S3. Ultrastructural analysis of MDA-MB-231 cells invading through Matrigel. (*A*) Composite of 24 separate transmission electron microscopy micrographs of a thin section across a MDA-MB-231 cell seeded in Matrigel. *Insets* 1–3 highlight differences in matrix structure (from less dense to more granular) in different positions of the matrix relative to the cell (boxed in *A*; 1, front of the cell; 2, side; and 3, behind the uropod). (*A′*) A higher magnification of the bleb-rich uropod region of the cell (dashed box in *A*). (*B*) Enlargement of the uropod region of another cell. Dashed lines (*A′* and *B*) point to the border between two regions with different matrix structure. Notice the constriction of the granular denser matrix region behind the bleb-rich uropod (arrows). Arrowheads point to blebs forming at the cell rear in a region of Matrigel with voids. [Scale bars, 10 μm (*A*), 2 μm (*A′*, *B*, and *Insets* 1–3).]

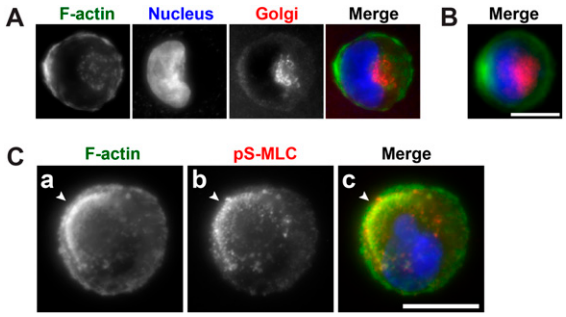

Fig. S4. Polarity of MDA-MB-231 cells in 3D Matrigel. (*A*) MDA-MB-231 cells were seeded in Matrigel, fixed after 4 h, and labeled for F-actin, the Golgi apparatus (CTR433 marker), and the nucleus (DAPI). A typical cell is shown with the nucleus (color-coded in blue in the merge image) close to the F-actin rich uropod (green), while the Golgi apparatus (red) is facing the front. (*B*) Superimposition of 15 cells aligned on the F-actin-rich uropod region revealing cell polarization. (Scale bar, 10 μm.) (*C*) MDA-MB-231 cells were plated atop a thick layer of Matrigel, and after 1 h, cells were fixed and stained for F-actin (*a*) and pS-MLC (*b*). In the merge image (*c*), F-actin is pseudocolored in green, pS-MLC in red, and the nucleus stained with DAPI is in blue. Note the presence of a uropod-like structure on the dorsal free surface of the cell opposite to the matrix (not visible). (Scale bar, 10 μm.)

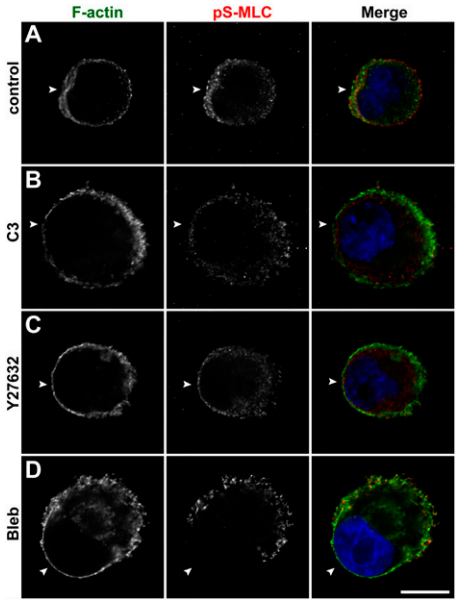

Fig. S5. Inhibition of actomyosin contractility impairs uropod formation. MDA-MB-231 cells were treated with C3 exoenzyme (C3, *B*), ROCK inhibitor Y27632 (*C*) or blebbistatin (bleb, *D*) and seeded in Matrigel in the presence of the drugs. After 4 h, cells were fixed and stained for F-actin (pseudocolored in green in the merge image, *Right*), pS-MLC (red) and for the nucleus (blue). In contrast to control cells that accumulate F-actin and pS-MLC in a uropod-like structure behind the nucleus (arrowhead, *A*), cells treated with the different drugs fail to form a uropod. (Scale bar, 10 μm.)

Table S1. Comparisons of mean velocity of siRNA or inhibitor-treated cells in 3D Matrigel with indicated controls

Cell populations	Speed, μm/h	SEM	*N*	*n*	*P* value (Dunnett test)	Versus
Mock	2.96	0.11	6	262		
siRhoA-a	1.69	0.15	2	93	$<10^{-9}$	Mock
sip34-b	2.63	0.12	2	77	N.S.	Mock
sib1-a	1.65	0.10	3	175	$<10^{-9}$	Mock
sib1-b	1.56	0.11	3	135	$<10^{-9}$	Mock
Control	3.22	0.14	4	121		
C3 exo.	1.71	0.18	3	103	$<10^{-9}$	Control
Y27632	0.52	0.05	3	126	$<10^{-9}$	Control
DMSO	2.83	0.12	5	196		
SMIFH2	1.83	0.09	3	183	$<10^{-9}$	DMSO
Bleb.	0.24	0.04	3	121	$<10^{-9}$	DMSO
GM6001	2.42	0.13	2	76	N.S.	DMSO
S36578-2	2.76	0.17	3	113	N.S	DMSO
Control ab.	3.92	0.33	2	54		
4B4	1.35	0.18	3	102	$<10^{-9}$	Control ab.

See Fig. 3*E*, filled bars. A nested (sample within condition) ANOVA followed by Dunnett's multiple comparisons to indicated control condition was used. Data are presented as mean ± SEM. *N*, number of independent experiments; *n*, total number of cells; N.S., not significant. $P < 0.05$ was considered statistically significant.

Table S2. Comparison of invasion of siRNA or inhibitor-treated cells through 3D Matrigel with indicated controls

Cell populations	% of invasion	SEM	*N*	*n*	*P* value (Bonferroni adjustment)	Versus
Mock	71.3	4.0	11	6,606		
siRhoA-a	6.1	1.4	6	3,466	$<10^{-9}$	Mock
siRhoA-b	3.5	1.1	2	681	$<10^{-9}$	Mock
sip34-A	83.0	2.7	3	2,200	N.S.	Mock
sip34-B	58.6	8.1	5	3,214	N.S.	Mock
Control	84.8	3.9	7	1,241		
C3 exoenzyme	23.4	6.6	3	482	$<10^{-6}$	Control
Y27632	1.9	1.1	4	1,367	$<10^{-7}$	Control
DMSO	78.0	7.7	3	458		
Blebbistatin	2.3	0.6	3	962	$<10^{-4}$	DMSO
Control ab.	64.5	9.5	3	639		
4B4	20.3	4.2	3	782	$<10^{-2}$	Control ab.

See Fig. 3*D*. A linear mixed-effects model was used on [% of invasion] to take into account a possible effect of experimental conditions (random part of the model), followed by multiple comparisons to control with the Bonferroni adjustment. A weight was applied to each value equal to the size of the sample (number of cells analyzed to obtain the value) divided by the mean size of samples in the same condition. Data are presented as weighted mean ± weighted SEM. *N*, number of independent experiments *n*, total number of cells; N.S., not significant. $P < 0.05$ was considered statistically significant.

Table S3. Comparisons of siRNA or inhibitor-treated cells with indicated controls for the presence of F-actin-rich uropod

Cell populations	Cells with uropod, %	SEM	*N*	*n*	*P* value (Dunnett test)	Versus
mock	83.5	1.7	6	297		
siRhoA-a	54.2	3.8	2	96	$<10^{-4}$	Mock
sip34-b	85.4	6.1	2	89	N.S.	Mock
sib1-a	45.9	3.8	3	181	$<10^{-5}$	Mock
sib1-b	42.9	1.6	3	154	$<10^{-5}$	Mock
control	84.8	3.3	4	165		
C3 exo.	38.0	11.9	3	108	$<10^{-2}$	Control
Y27632	2.2	1.3	3	139	$<10^{-4}$	Control
DMSO	81.1	3.3	5	228		
SMIFH2	47.0	4.6	3	196	$<10^{-3}$	DMSO
Bleb.	4.1	1.9	2	97	$<10^{-6}$	DMSO
GM6001	77.8	7.5	2	81	N.S.	DMSO
S36578-2	76.6	1.9	3	128	N.S.	DMSO
control ab.	80.3	9.1	2	66		
4B4	38.3	5.1	3	115	0.021	Control ab.

See Fig. 3*E*, open bars. A one-way ANOVA was performed on [% of cells with uropod], followed by multiple comparisons to control by the Dunnett test. A weight was applied to each value equal to the size of the sample (number of cells analyzed to obtain the value) divided by the mean size of samples in the same condition. Data are presented as weighted mean ± weighted SEM. *N*, number of independent experiments; *n*, total number of cells; N.S., not significant. $P < 0.05$ was considered statistically significant.

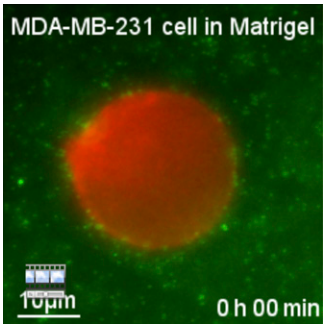

Movie S1. Matrigel remodeling caused by MDA-MB-231 round cell migration. Time-series movie of MDA-MB-231 cell stably expressing mCh-Lifeact moving within 3D Matrigel seeded with fluorescent microbeads. The video was acquired by wide-field fluorescence microscopy at 15-min intervals during 2 h by alternating two channels to register the signals for the Factin probe mCh-Lifeact (red) and the microbeads (green). The last part of the movie shows the 2-h time projection of the microbead time-series superimposed with the last frame of the mCh-Lifeact sequence.

Movie S1

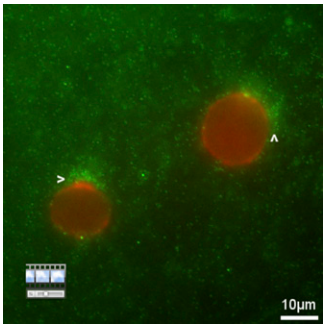

Movie S2. Beads accumulate at the rear of MDA-MB-231 cells moving within 3D Matrigel. Time-series movie of MDA-MB-231 cells expressing mCh-Lifeact within 3D Matrigel seeded with fluorescent microbeads as in Movie S1 (timepoints are 15 min apart). Video shows progressive accumulation of microbeads behind the F-actin-rich rear of the cells during migration (arrowheads).

Movie S2

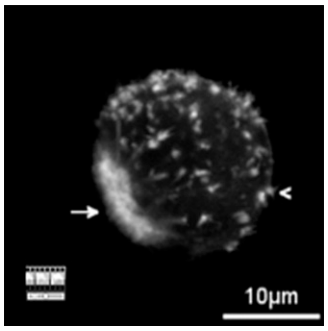

Movie S3. F-actin organization in MDA-MB-231 cell in 3D Matrigel. MDA-MB-231 cell stably expressing the F-actin probe mCh-Lifeact was seeded in 3D Matrigel and a stack of optical sections was recorded by confocal spinning disk microscopy. The movie shows a 360 ° rotation around the cell. The arrow points to the F-actin-rich uropod; the arrowhead depicts invadopodia-like structures protruding from the cell surface.

Movie S3

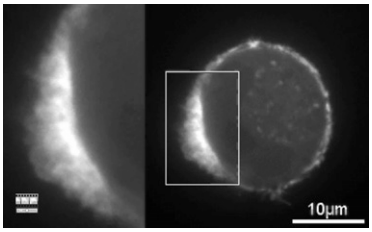

Movie S4. The uropod-like region is a site of intense blebbing activity. Typical time-lapse of mCh-Lifeact MDA-MB-231 cell seeded in Matrigel and imaged by confocal spinning disk microscopy to show intense blebbing activity at the uropod (timepoints are 10 s apart). The boxed region is zoomed out on the left side of the movie. Arrowheads point to F-actin bundles extending radially from the uropod toward the cell cortex.

Movie S4

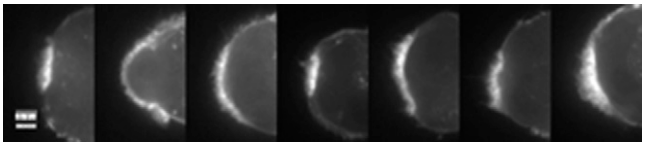

Movie S5. Large blebs form at the edge of the uropod. Gallery of time-lapse sequences of the uropod region of mCh-Lifeact MDA-MB-231 cells seeded in Matrigel (timepoints are 10 s apart). Larger blebs form at the edge of the uropod.

Movie S5

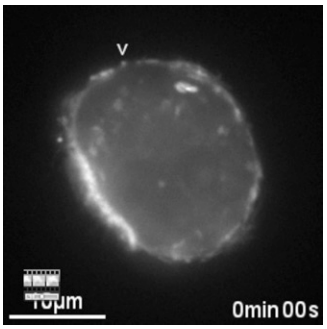

Movie S6. Reward movement of the actin cortex toward uropod. Time-lapse of mCh-Lifeact MDA-MB-231 cell seeded in Matrigel and imaged by confocal spinning disk microscopy (timepoints are 10 s apart). The cell was repositioned to appear static over time. Arrowhead points to a cortical invadopodia-like structure with convergent retrograde movement toward the uropod.

Movie S6

Movie S7. Vertical invasion in Matrigel occurs through uropod formation. Z-stack of an MDA-MB-231 cell fixed and stained for F-actin, pS-MLC, and the nucleus 1 h after plating atop a thick layer of Matrigel. The movie shows a stack of optical sections of confocal spinning disk microscopy recorded from the invasive ventral surface of the cells in contact with Matrigel (not visible) to the free dorsal surface. The arrowhead points to the uropod located opposite to the invasive ventral surface.

Movie S7

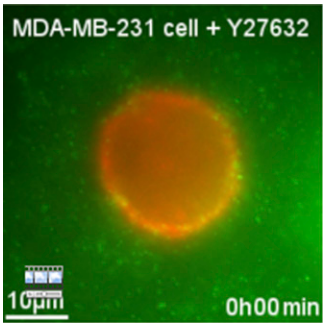

Movie S8. Time-lapse movie of mCh-Lifeact MDA-MB-231 cell in 3D Matrigel treated with 10 µM Y27632. Timepoints are 15 min apart. The last part of the movie shows the 4-h time projection of the microbead time-series superimposed with the last frame of the mCh-Lifeact sequence.

Movie S8

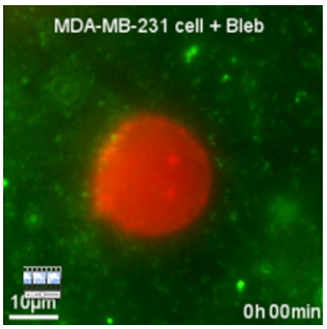

Movie S9. Time-lapse movie of mCh-Lifeact MDA-MB-231 cell in 3D Matrigel treated with 50 μM blebbistatin. Same as in Movie S8.

Movie S9

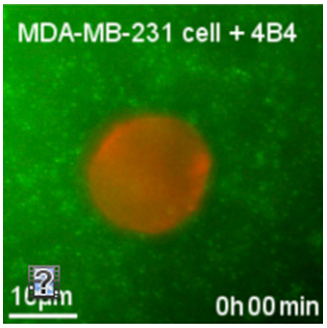

Movie S10. Time-lapse movie of mCh-Lifeact MDA-MB-231 cell in 3D Matrigel treated with 2 μg/mL 4B4 anti-β1 integrin blocking antibody. Same as in Movie S8. Some migration (~30–40% of control cell speed) is retained by 4B4-treated cells, which loose their contacts with the matrix (see area devoid of beads on left side).

Movie S10

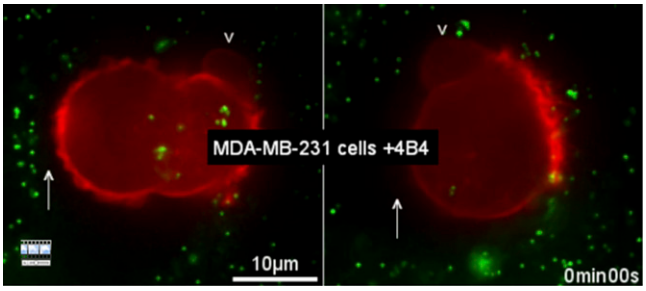

Movie S11. Time-lapse movies of mCh-Lifeact MDA-MB-231 cells in 3D Matrigel treated with 2 μg/mL 4B4 anti-β1 integrin blocking antibody. Timepoints are 10 s apart. White arrowhead points to large blebs forming in the middle plane of the cells, in regions of cell constriction (yellow arrowhead).

Movie S11